*electronics*

MDPI

*Article*

# A New Study on the Temperature and Bias Dependence of the Kink Effects in $S_{22}$ and $h_{21}$ for the GaN HEMT Technology

**Giovanni Crupi [1,*], Antonio Raffo [2], Valeria Vadalà [2], Giorgio Vannini [2] and Alina Caddemi [3]**

[1] Department of Biomedical and Dental Sciences and Morphofunctional Imaging, University of Messina, 98125 Messina, Italy
[2] Department of Engineering, University of Ferrara, 44122 Ferrara, Italy; antonio.raffo@unife.it (A.R.); vdlvlr@unife.it (V.V.); giorgio.vannini@unife.it (G.V.)
[3] Department of Engineering, University of Messina, 98166 Messina, Italy; acaddemi@unime.it
* Correspondence: crupig@unime.it; Tel.: +39-090-3977327

Received: 16 October 2018; Accepted: 21 November 2018; Published: 25 November 2018


**Abstract:** The aim of this feature article is to provide a deep insight into the origin of the kink effects affecting the output reflection coefficient ($S_{22}$) and the short-circuit current-gain ($h_{21}$) of solid-state electronic devices. To gain a clear and comprehensive understanding of how these anomalous phenomena impact device performance, the kink effects in $S_{22}$ and $h_{21}$ are thoroughly analyzed over a broad range of bias and temperature conditions. The analysis is accomplished using high-frequency scattering (*S*-) parameters measured on a gallium-nitride (GaN) high electron-mobility transistor (HEMT). The experiments show that the kink effects might become more or less severe depending on the bias and temperature conditions. By using a GaN HEMT equivalent-circuit model, the experimental results are analyzed and interpreted in terms of the circuit elements to investigate the origin of the kink effects and their dependence on the operating condition. This empirical analysis provides valuable information, simply achievable by conventional instrumentation, that can be used not only by GaN foundries to optimize the technology processes and, as a consequence, device performance, but also by designers that need to face out with the pronounced kink effects of this amazing technology.

**Keywords:** equivalent circuit; GaN; HEMT; scattering parameter measurements; solid-state electronic device

## 1. Introduction

With the aim of enabling microwave engineers to exploit advanced transistor technologies at their best, increasing attention is being given to the investigation of the kink effects in the output reflection coefficient ($S_{22}$) and the short-circuit current-gain ($h_{21}$) of solid-state electronic devices made with different semiconductor materials, like silicon (Si), gallium arsenide (GaAs), and gallium nitride (GaN) [1–13]. The kink in $S_{22}$ consists in the change of the concavity of the function Im($S_{22}$) versus Re($S_{22}$) (i.e., from convex to concave and vice versa), while the kinks in $h_{21}$ consist of peaks that are detectable by plotting the magnitude of $h_{21}$ in dB versus the frequency on a log scale. As the kink effects can be interpreted in terms of the transistor equivalent-circuit elements, many studies have been developed to identify those ones playing a dominant role, depending on the specific case study. The origin of the kink effect in $S_{22}$ has been mostly ascribed to high values of the transconductance ($g_m$) [1,4–6], whereas $h_{21}$ can be affected by a first kink, originating from the resonance between the extrinsic inductances and the intrinsic capacitances [7–9,12,13], and a second kink, arising from the

resonance of the extrinsic reactive elements [12,13]. It is worth underlining that an accurate study of the kink effects in $S_{22}$ and $h_{21}$ parameters of microwave transistors represents a powerful tool for microwave engineers for fabrication, modeling and design purposes. Device technologists might enhance or alleviate the kinks in $S_{22}$ and $h_{21}$, depending on the application constraints, simply through optimization of the device layout and structure. Device modelers can exploit the kinks in $S_{22}$ and $h_{21}$ for extracting equivalent circuit parameters (e.g., the resonance frequency associated with the first kink in $h_{21}$ has been used to accomplish the challenging task of determining the intrinsic output capacitance [7,8]). Circuit designers should properly take into account the kink effect in $S_{22}$, especially for the design of broadband output matching networks [14,15]. In addition, circuit designers can benefit from the kinks in $h_{21}$ as they enable achieving an increase in the current gain at the resonant frequencies. However, so far, the interest in obtaining active transistor operation at frequencies beyond the cut-off frequency ($f_T$) has been focused on bipolar transistors (e.g., by proper design of the so-called resonance phase transistor [16–21]), recent studies have shown that the achievement of a current gain even at frequencies higher than $f_T$ is achievable also in FET transistors, owing to the kinks in $h_{21}$ [12,13].

This feature article is focused on investigating the kinks in $S_{22}$ and $h_{21}$ for the gallium-nitride (GaN) high electron-mobility transistor (HEMT) technology, which is receiving increasing attention for high-temperature and high-power applications at high frequencies [22–29]. In particular, the kinks are studied at different ambient (i.e., case) temperatures ($T_a$) and bias voltages ($V_{GS}$ and $V_{DS}$). The study consists of a comprehensive examination of the experimental results based on scattering (*S*-) parameter measurements and an exhaustive interpretation of the achieved findings using the transistor equivalent-circuit model. Although GaN HEMT is used as a case study, the reported study is technology-independent as it is based on a standard equivalent circuit topology for FETs, thus making the achieved finding representative and generalizable for any FET. This is confirmed by previous studies which have already demonstrated that the appearance or absence of the kinks in $S_{22}$ and $h_{21}$ is simply rooted in the values of the equivalent circuit elements of the tested FET, besides the analyzed frequency range [1,6,9,12,13].

The remainder of this article is organized as follows. Section 2 is devoted to the analysis of the kink effect in $S_{22}$; Section 3 is focused on the investigation of the kink effects in $h_{21}$; and Section 4 summaries the main conclusions.

## 2. Kink Effect in $S_{22}$

The studied solid-state electronic device is a GaN HEMT with a gate length of 0.25 µm and a gate width of 1.5 mm (i.e., 10 × 150 µm) (see Figure 1a). It was manufactured in the GH25-10 technology by United Monolithic Semiconductors (UMS) [30–32], using an AlGaN/GaN heterostructure grown on silicon carbide (SiC) substrate with a field plate for power applications. This foundry process, entitling a power density of 4.5 W/mm with typical $f_T$ of 25 GHz, is optimized for X-band (i.e., 8–12 GHz) high-power applications. The *S*-parameters were measured from 0.2 to 65 GHz under different bias conditions and at four ambient temperatures: 35 °C, 90 °C, 145 °C, and 200 °C. Subsequently, the $h_{21}$ parameter was straightforwardly calculated from the measured *S*-parameters by using conventional transformation formulas [33]. Figure 1b shows the small-signal equivalent circuit used for modelling the tested transistor. Firstly, the extrinsic elements were determined from *S*-parameters at "cold" pinch-off condition (i.e., $V_{DS}$ = 0 V and $V_{GS}$ = −4 V) and, subsequently, the intrinsic elements were calculated from the intrinsic admittance (*Y*-) parameters at each bias point [12].

Figures 2 and 3 show the *S*-parameters measured at the four investigated ambient temperatures with $V_{DS}$ = 30 V and for two values of $V_{GS}$: −3.5 V and −3.1 V, respectively. It can be observed that $S_{22}$ of the tested device is affected by the kink effect under both bias conditions. As illustrated in Figures 2 and 3, the kink effect can be detected also as a dip in the magnitude of $S_{22}$, due to two zeros occurring between two poles. This is in line with findings from previous studies showing that the kink effect in $S_{22}$ can be analyzed also in terms of poles and zeros [2–4,6]. The shape of the kink effect strongly depends on the combined effects of equivalent circuit elements whose values

might remarkably vary with the operating conditions. By heating the device, the kink effect gets less pronounced and this can be attributed to the reduction of $g_m$ which is associated to a decrease of the average velocity of the electrons drifting in the 2-D electron gas (2DEG) channel. As a matter of fact, $g_m$ plays a dominant role in determining the appearance and the shape of the kink effect in $S_{22}$. A higher temperature leads also to a decrease in the drain-source resistance ($R_{ds}$), moving the starting point of $S_{22}$ closer to the short-circuit condition. By increasing $T_a$ from 35 °C to 200 °C when $V_{GS}$ is −3.5 V, $g_m$ and $R_{ds}$ decrease from 225.7 to 186.8 mS and from 189.7 to 146.7 Ω, respectively. Given the same increase in $T_a$ but with $V_{GS}$ = −3.1 V, $g_m$ and $R_{ds}$ decrease from 347.9 to 215.4 mS and from 138.9 to 135.2 Ω, respectively.

The reduction of $g_m$ and $R_{ds}$ at higher temperatures can be, respectively, noticed from the decrease in the low-frequency magnitudes of the forward transmission ($S_{21}$) and reflection coefficient $S_{22}$ (see Figures 2e,f and 3e,f), since at relatively low frequencies $S_{21}$ and $S_{22}$ can be linked to $g_m$ and $R_{ds}$ as follows [34]:

$$S_{21} = -2g_{mExtr}(R_0 // R_{dsExtr}) \quad (1)$$

$$S_{22} = \frac{R_{dsExtr} - R_0}{R_{dsExtr} + R_0} \quad (2)$$

$$g_{mExtr} = \frac{g_m}{1 + g_m R_s + R_{ds}^{-1}(R_s + R_d)} \quad (3)$$

$$R_{dsExtr}^{-1} = \frac{R_{ds}^{-1}}{1 + g_m R_s + R_{ds}^{-1}(R_s + R_d)} \quad (4)$$

where $R_0$ is the characteristic resistance (i.e., 50 Ω), while $g_{mExtr}$ and $R_{dsExtr}$ represent the extrinsic transconductance and drain-source resistance.

To focus attention on the $V_{GS}$ dependence, Figure 4 illustrates the *S*-parameters measured at $T_a$ = 35 °C, $V_{DS}$ = 30 V and with $V_{GS}$ equal to −3.5 V and −3.1 V. By varying $V_{GS}$ from −3.5 to −3.1 V, the improvement of $g_m$ leads to an increase of the low-frequency magnitude of $S_{21}$ and to an enhancement of the kink effect in $S_{22}$, whereas the decrease of $R_{ds}$ leads to a shift of the starting point of $S_{22}$ towards the short-circuit condition.

As can be observed in Figure 5, the kink effect in $S_{22}$ vanishes when $V_{DS}$ reaches 0 V and, in line with this finding, the dip in the magnitude of $S_{22}$ disappears. This is because, by reducing $V_{DS}$, $g_m$ decreases and, in addition, its role is further diminished by the decrease of $R_{ds}$. As a matter of fact, $R_{ds}$ is connected in parallel with the voltage-controlled current source (i.e., $g_m e^{-j\omega\pi m}$V) and thus its reduction tends to short circuit the contribution of $g_m$, thereby contributing to the suppression of the kink effect in $S_{22}$ and to the decrease in the low-frequency magnitude of $S_{21}$ (see Equation (1)). The reduction of $g_m$ and $R_{ds}$ at lower $V_{DS}$ can be, respectively, noticed from the decrease in the low-frequency magnitude of $S_{21}$ (see Figure 5e) and the shift of the starting point of $S_{22}$ closer to the short-circuit condition (see Figure 5d).

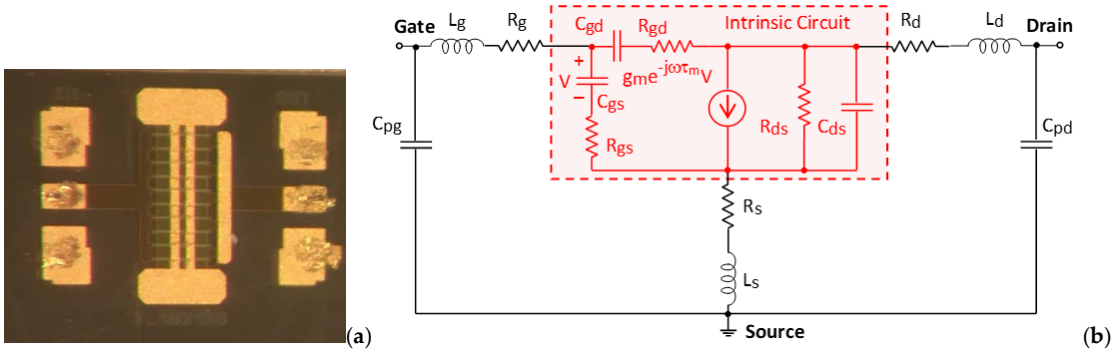


**Figure 1.** (**a**) Photograph of the studied GaN HEMT and (**b**) its small-signal equivalent circuit.

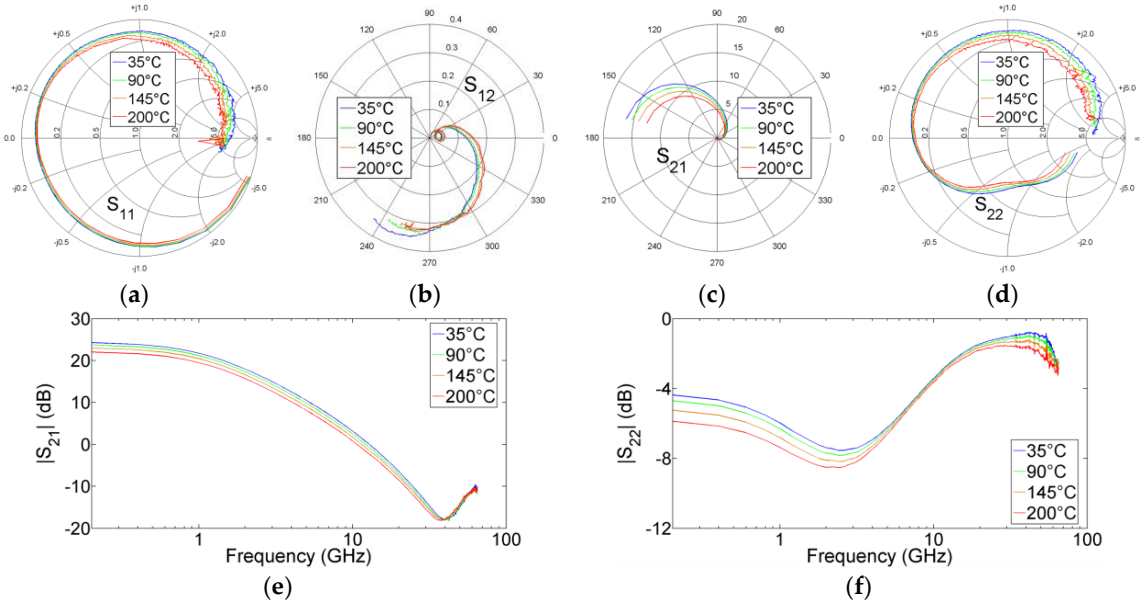


**Figure 2.** Measured (**a**) $S_{11}$, (**b**) $S_{12}$, (**c**) $S_{21}$, (**d**) $S_{22}$, (**e**) magnitude of $S_{21}$, and (**f**) magnitude of $S_{22}$ from 0.2 to 65 GHz for a GaN HEMT at $V_{DS}$ = 30 V and $V_{GS}$ = −3.5 V under four ambient temperatures: 35 °C, 90 °C, 145 °C, and 200 °C.

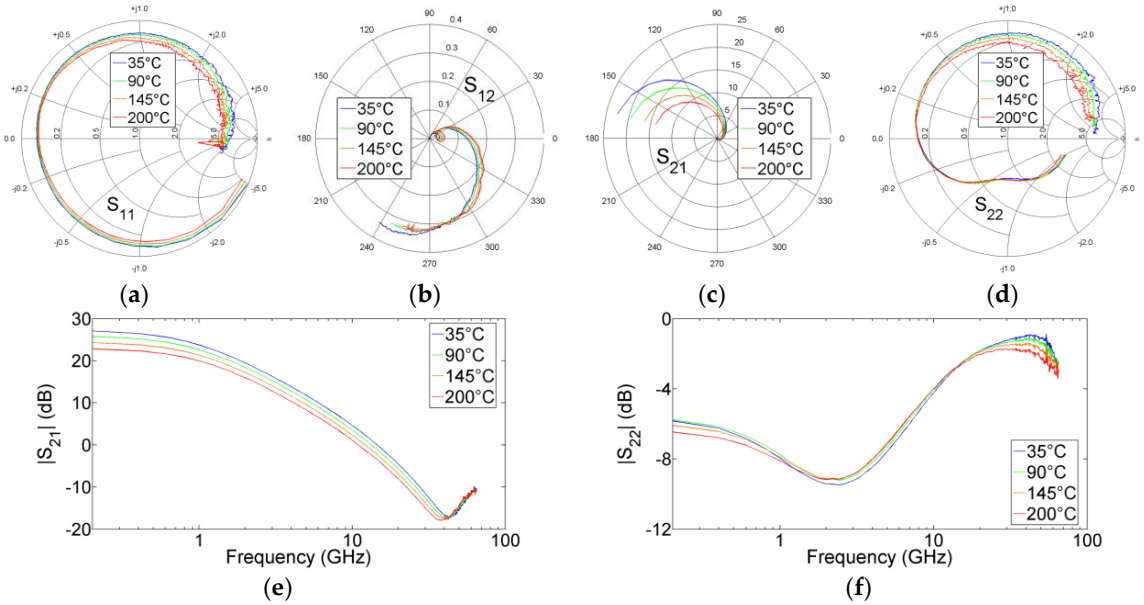


**Figure 3.** Measured (**a**) $S_{11}$, (**b**) $S_{12}$, (**c**) $S_{21}$, (**d**) $S_{22}$, (**e**) magnitude of $S_{21}$, and (**f**) magnitude of $S_{22}$ from 0.2 to 65 GHz for a GaN HEMT at $V_{DS}$ = 30 V and $V_{GS}$ = −3.1 V under four ambient temperatures: 35 °C, 90 °C, 145 °C, and 200 °C.

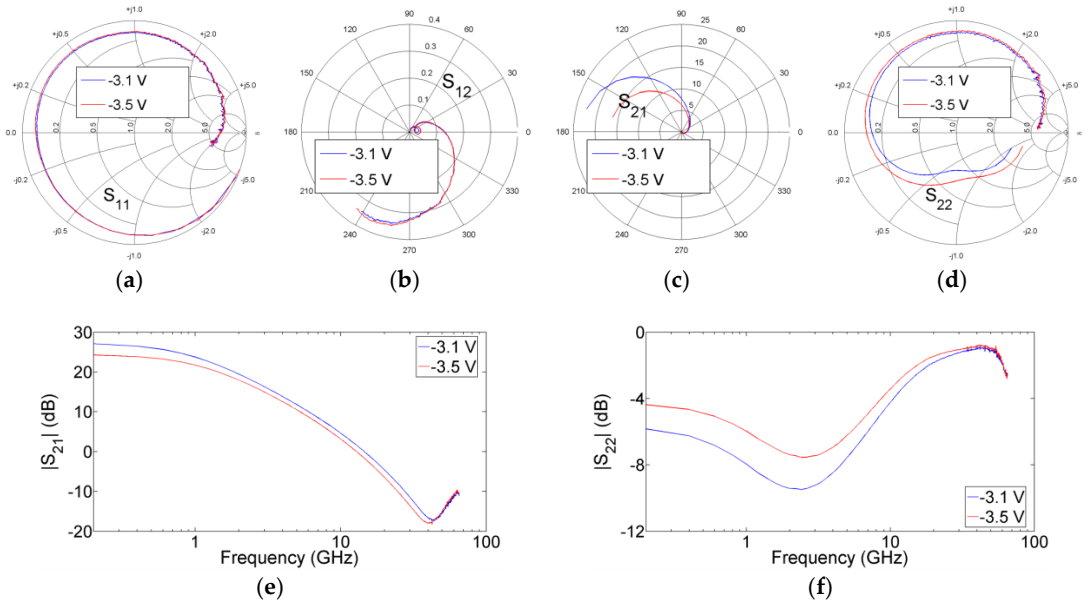


**Figure 4.** Measured (**a**) $S_{11}$, (**b**) $S_{12}$, (**c**) $S_{21}$, (**d**) $S_{22}$, (**e**) magnitude of $S_{21}$, and (**f**) magnitude of $S_{22}$ from 0.2 to 65 GHz for a GaN HEMT at $T_a$ = 35 °C and $V_{DS}$ = 30 V for two values of $V_{GS}$: −3.5 V and −3.1 V.

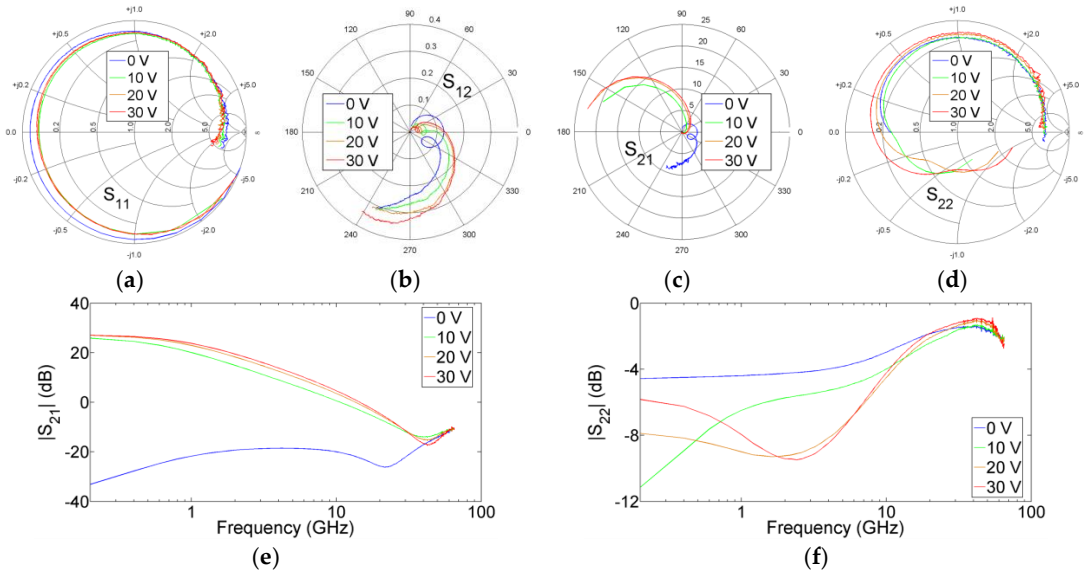


**Figure 5.** Measured (**a**) $S_{11}$, (**b**) $S_{12}$, (**c**) $S_{21}$, (**d**) $S_{22}$, (**e**) magnitude of $S_{21}$, and (**f**) magnitude of $S_{22}$ from 0.2 to 65 GHz for a GaN HEMT at $T_a$ = 35 °C and $V_{GS}$ = −3.1 V for four values of $V_{DS}$: 0 V, 10 V, 20 V, and 30 V. $S_{21}$ at $V_{DS}$ = 0 V is multiplied by a factor of 30 in Figure 4c for better readability.

Figure 6a reports the comparison between measured and simulated $S_{22}$ at $T_a$ = 35 °C, $V_{DS}$ = 30 V, and $V_{GS}$ = −3.1 V. Although the extraction of a model that can faithfully reproduce the behavior of a device with a large gate periphery over a broad frequency range reaching very high frequencies is quite a challenging task, the standard equivalent-circuit model is able to mimic the general trend of the measurements and, in particular, to predict the kink in $S_{22}$ and the dip in its magnitude too (see Figure 6b). Furthermore, as will be seen in the next section, the extracted model also allows the prediction of the two kinks in $h_{21}$. It is worth noticing that, in accordance with what is stated above, the kink effect in the simulated $S_{22}$ can be suppressed by reducing $g_m$ and/or $R_{ds}$ (see Figure 6c–f). This is because $S_{22}$ becomes kink-free by nullifying the value of $g_m$ and/or its contribution. On the other hand, by increasing $R_{ds}$ at a very high value, the shape of $S_{22}$ is modified somewhat and the

starting point of $S_{22}$ shifts towards the open-circuit condition but with the kink effect still affecting $S_{22}$ (see Figure 6g,h). It is worth noticing that although changing only one element of the model might be not physically representative of a real device, repeating this type of analysis enables understanding of how each element impacts on the appearance and shape of the kinks and the physical soundness of the achieved outcomes is guaranteed by the fact that the equivalent-circuit model is a physically meaningful representation of the FET behavior. As an example, this type of powerful analysis has been conducted in a pioneering study to explore the origin of the kink effect in $S_{22}$ by varying the intrinsic element values, showing that $g_m$ plays a dominant role [1].

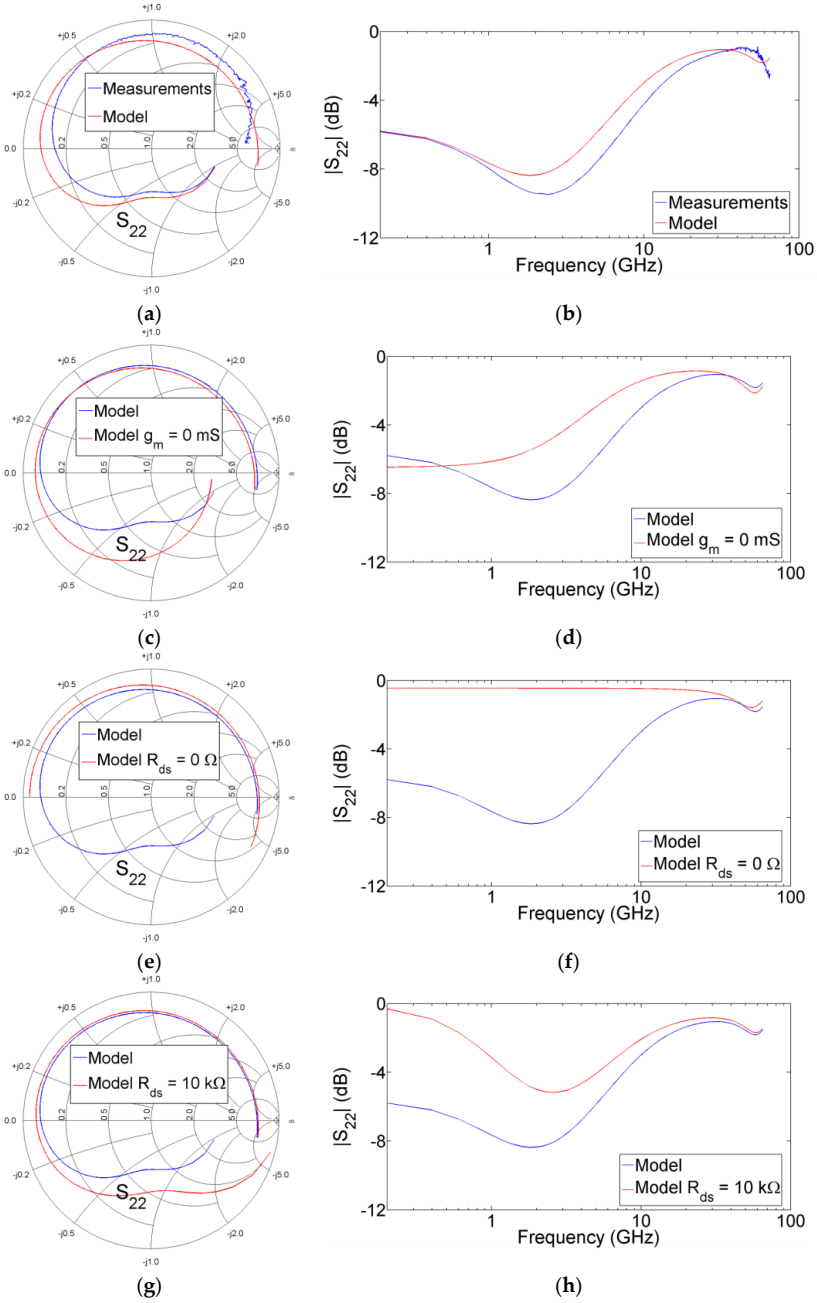


**Figure 6.** Comparison between measured and simulated (**a**) $S_{22}$ and (**b**) its magnitude from 0.2 to 65 GHz for a GaN HEMT at $T_a$ = 35 °C, $V_{DS}$ = 30 V, and $V_{GS}$ = −3.1 V. The values of $g_m$ and $R_{ds}$ for the extracted equivalent-circuit model are 347.9 mS and 138.9 Ω, respectively. The simulated $S_{22}$ is compared with the simulations achieved by using the models with: (**c**,**d**) $g_m$ = 0 mS, (**e**,**f**) $R_{ds}$ = 0 Ω, and (**g**,**h**) $R_{ds}$ = 10 kΩ.

As is well known, the most popular technique for determining the extrinsic circuit elements for FETs is based on using *S*-parameters measured under "cold" conditions ($V_{DS}$ = 0 V, i.e., passive device) [35–39]. As there are no electrons drifting from source to drain when $V_{DS}$ = 0 V, $g_m$ is equal to zero, thus implying that $S_{21}$ becomes equal to $S_{12}$ and $S_{22}$ turns out to be kink-free. This is illustrated in Figure 7, showing *S*-parameters measured at two typical bias points used for modeling purpose: "cold" unbiased (i.e., $V_{GS}$ = 0 V) and pinched-off (i.e., $V_{GS}$ = −4 V) conditions. By moving from an open-channel to pinch-off condition, the starting point of $S_{22}$ shifts from the short-circuit to the open-circuit condition (see Figure 7d), owing to the increase of $R_{ds}$, but without the occurrence of the kink effect as $g_m$ is kept at zero by biasing the device under "cold" condition.

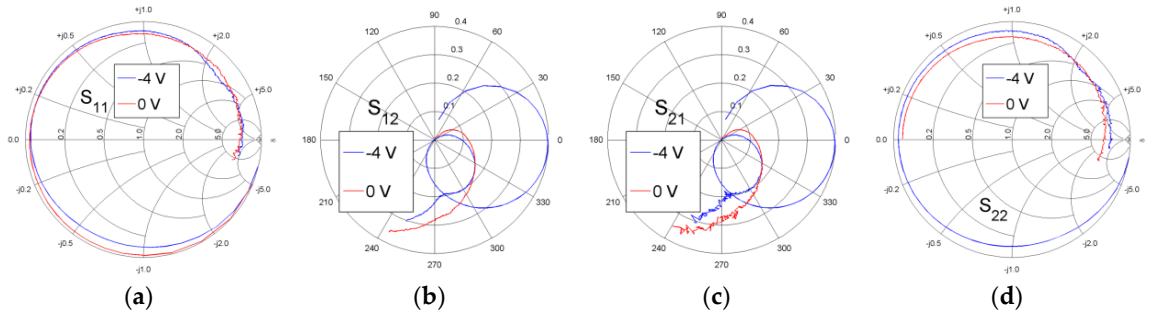


**Figure 7.** Measured (**a**) $S_{11}$, (**b**) $S_{12}$, (**c**) $S_{21}$, and (**d**) $S_{22}$ from 0.2 to 65 GHz for a GaN HEMT at $T_a$ = 35 °C and $V_{DS}$ = 0 V for two values of $V_{GS}$: −4 V and 0 V.

## 3. Kink Effects in $h_{21}$

Figures 8 and 9 report the measured $h_{21}$ at the four investigated ambient temperatures with $V_{DS}$ = 30 V and for two values of $V_{GS}$: −3.5 V and −3.1 V, respectively. It is found that two peaks appear in $h_{21}$ at each bias condition. It has already been demonstrated in previous works that the first peak is due to the resonance between the extrinsic inductances and the intrinsic capacitances [7–9,12,13], whereas the second peak is due to the resonance of the extrinsic inductive and capacitive contributions [12,13]. The experiments show that the second peak is substantially insensitive to $T_a$, as expected considering that the extrinsic reactive elements are mostly temperature-independent, and the first peak is roughly independent of $T_a$, consistently with the slight temperature dependence of the intrinsic capacitances.

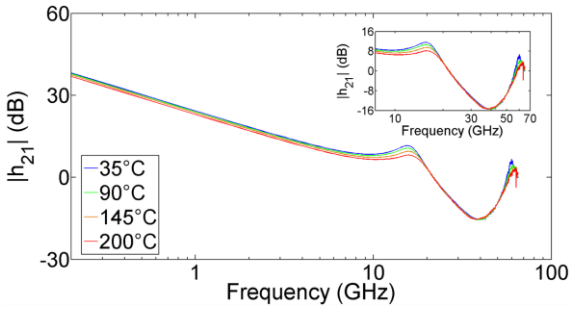


**Figure 8.** Measured $h_{21}$ from 0.2 to 65 GHz for a GaN HEMT at $V_{DS}$ = 30 V and $V_{GS}$ = −3.5 V under four ambient temperatures: 35 °C, 90 °C, 145 °C, and 200 °C.

To focus attention on the $V_{GS}$ dependence, Figure 10 illustrates $h_{21}$ measured at $T_a$ = 35 °C, $V_{DS}$ = 30 V and with $V_{GS}$ equal to −3.5 V and −3.1 V. By varying $V_{GS}$ from −3.5 to −3.1 V, the improvement of $g_m$ leads to an increase of the low-frequency magnitude of $h_{21}$ but the two peaks are mostly insensitive to this variation of $V_{GS}$.

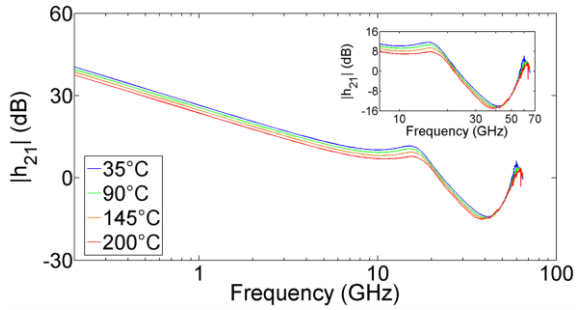


**Figure 9.** Measured $h_{21}$ from 0.2 to 65 GHz for a GaN HEMT at $V_{DS}$ = 30 V and $V_{GS}$ = −3.1 V under four ambient temperatures: 35 °C, 90 °C, 145 °C, and 200 °C.

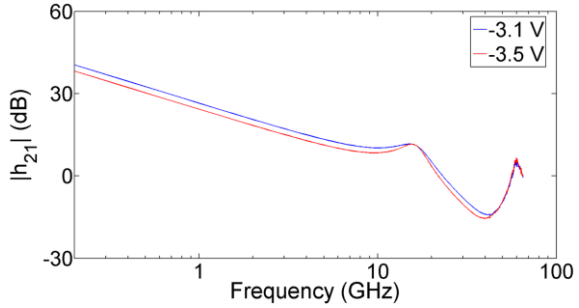


**Figure 10.** Measured $h_{21}$ from 0.2 to 65 GHz for a GaN HEMT at $T_a$ = 35 °C and $V_{DS}$ = 30 V for two values of $V_{GS}$: −3.5 V and −3.1 V.

As can be observed in Figure 11, the first peak disappears at zero $V_{DS}$, owing to the reduction of $R_{ds}$ that tends to short circuit the intrinsic capacitive contributions [7,9,12]. On the other hand, the second peak is mostly insensitive to $V_{DS}$, owing to the bias independence of the extrinsic reactive elements [12].

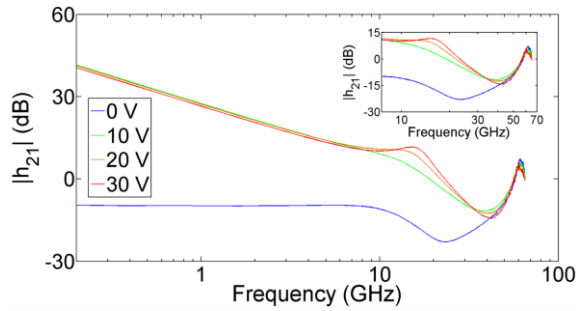


**Figure 11.** Measured $h_{21}$ from 0.2 to 65 GHz for a GaN HEMT at $T_a$ = 35 °C and $V_{GS}$ = −3.1 V for four different values of $V_{DS}$: 0 V, 10 V, 20 V, and 30 V.

Figure 12a reports the comparison between measured and simulated $h_{21}$ at $T_a$ = 35 °C, $V_{DS}$ = 30 V, and $V_{GS}$ = −3.1 V. As can be observed, the standard equivalent-circuit model is able to predict the two peaks in $h_{21}$. Figure 12b illustrates that a reduction of $g_m$ results in a dramatic degradation of the low-frequency magnitude of $h_{21}$ but with the two peaks still affecting $h_{21}$. It is worth noticing that the first kink effect in the simulated $h_{21}$ vanishes by reducing $R_{ds}$ to zero (see Figure 12c), whereas $h_{21}$ is substantially insensitive to an increase of $R_{ds}$ (see Figure 12d).

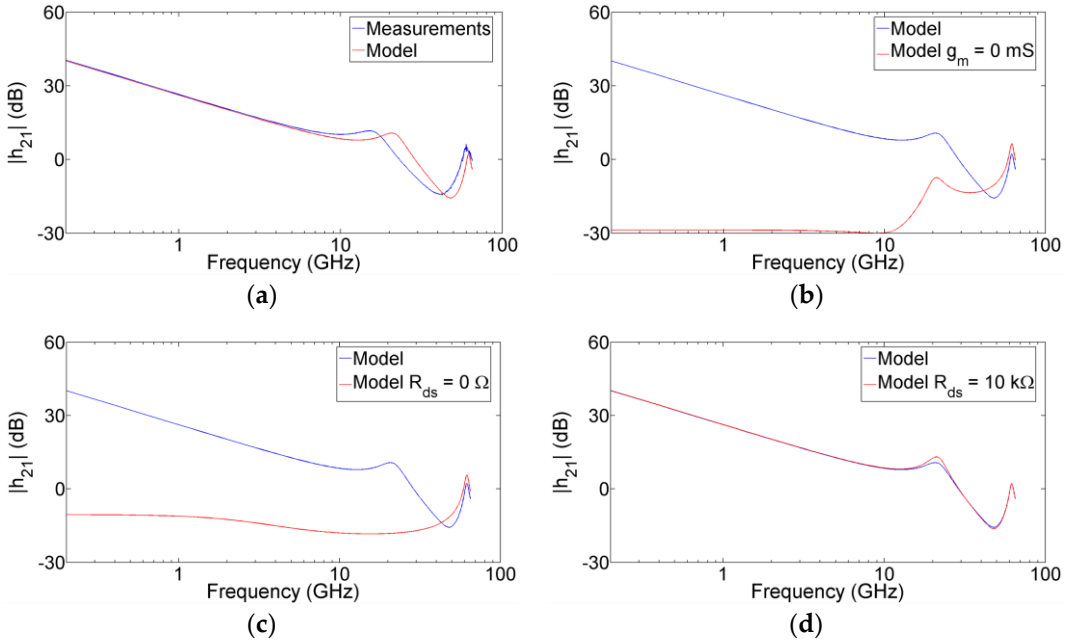


**Figure 12.** Comparison between measured and simulated (**a**) $h_{21}$ from 0.2 to 65 GHz for a GaN HEMT at $T_a$ = 35 °C, $V_{DS}$ = 30 V, and $V_{GS}$ = −3.1 V. The values of $g_m$ and $R_{ds}$ for the extracted equivalent-circuit model are 347.9 mS and 138.9 Ω, respectively. The simulated $h_{21}$ is compared with the simulations achieved by using the models with: (**b**) $g_m$ = 0 mS, (**c**) $R_{ds}$ = 0 Ω, and (**d**) $R_{ds}$ = 10 kΩ.

## 4. Conclusions

We have reported a thorough and critical investigation of the kinks in $S_{22}$ and $h_{21}$ parameters for solid-state electronic devices. To gain a comprehensive and in-depth understanding of their origin, we have developed a measurement-based analysis focusing on a GaN HEMT as a case study. However, the achieved outcomes can be straightforwardly generalized to other FET types, since a standard topology of FET equivalent circuit has been successfully used for analyzing and comprehending the experiments. We have shown that the kink in $S_{22}$ depends on both temperature and bias conditions, the first peak in $h_{21}$ depends slightly on temperature and strongly on bias conditions, and the second peak in $h_{21}$ is substantially bias- and temperature-insensitive. We have reported an exhaustive interpretation of the experimental findings by using a standard transistor equivalent-circuit model as it allows capturing all the three observed kinks. The origin of the kink effect in $S_{22}$ is mostly due to a high value of $g_m$, the first peak in $h_{21}$ originates from the resonance between the extrinsic inductances and the intrinsic capacitances, and the second kink in $h_{21}$ originates from the resonance of the extrinsic inductive and capacitive contributions. A reduction of $g_m$ allows only suppression of the kink effect in $S_{22}$, while a reduction of $R_{ds}$ leads to the suppression of the kink effect in $S_{22}$ and the first peak in $h_{21}$ by short circuiting the contributions of $g_m$ and intrinsic capacitances. On the other hand, it has been shown that the second peak in $h_{21}$ still occurs, independently of the reduction of $g_m$ and $R_{ds}$.

**Author Contributions:** Investigation, G.C. and V.V.; Methodology, G.C. and A.R.; Supervision, G.V. and A.C.; Writing–original draft, G.C.; Writing–review & editing, A.R., V.V., G.V. and A.C.

**Funding:** This research was funded in part by the Eurostars project E!10149 MicromodGaN.

**Conflicts of Interest:** The authors declare no conflict of interest.

## References

1. Lu, S.-S.; Meng, C.; Chen, T.-W.; Chen, H.-C. The origin of the kink phenomenon of transistor scattering parameter $S_{22}$. *IEEE Trans. Microw. Theory Tech.* **2001**, *49*, 333–340. [CrossRef]

2. Lu, S.-S.; Meng, C.; Chen, T.-W.; Chen, H.-C. A novel interpretation of transistor S-parameters by poles and zeros for RF IC circuit design. *IEEE Trans. Microw. Theory Tech.* **2001**, *49*, 406–409. [CrossRef]
3. Lin, Y.-S.; Lu, S.-S. An analysis of the kink phenomenon of scattering parameter $S_{22}$ in RF power mosfets for system-on-chip (SOC) applications. *Microw. Opt. Technol. Lett.* **2003**, *36*, 371–376. [CrossRef]
4. Lin, Y.-S. Temperature dependence of the power gain and scattering parameters $S_{11}$ and $S_{22}$ of an RF nMOSFET with advanced RF-CMOS technology. *Microw. Opt. Technol. Lett.* **2005**, *44*, 180–185. [CrossRef]
5. Crupi, G.; Avolio, G.; Raffo, A.; Barmuta, P.; Schreurs, D.M.M.-P.; Caddemi, A.; Vannini, G. Investigation on the thermal behavior for microwave GaN HEMTs. *Solid-State Electron.* **2011**, *64*, 28–33. [CrossRef]
6. Crupi, G.; Raffo, A.; Caddemi, A.; Vannini, G. The kink phenomenon in the transistor $S_{22}$: A systematic and numerical approach. *IEEE Microw. Wirel. Comp. Lett.* **2012**, *22*, 406–408. [CrossRef]
7. Crupi, G.; Raffo, A.; Schreurs, D.M.M.-P.; Avolio, G.; Caddemi, A.; Vannini, G. A clear-cut understanding of the current-gain peak in HEMTs: Theory and experiments. *Microw. Opt. Technol. Lett.* **2012**, *54*, 2801–2806. [CrossRef]
8. Crupi, G.; Raffo, A.; Schreurs, D.M.M.-P.; Avolio, G.; Caddemi, A.; Vannini, G. Identification of the intrinsic capacitive core for GaAs HEMTs by investigating the frequency behavior of the impedance parameters. *Microw. Opt. Technol. Lett.* **2013**, *55*, 1237–1240. [CrossRef]
9. Crupi, G.; Raffo, A.; Marinković, Z.; Avolio, G.; Caddemi, A.; Marković, V.; Vannini, G.; Schreurs, D.M.M.-P. An extensive experimental analysis of the kink effects in $S_{22}$ and $h_{21}$ for a GaN HEMT. *IEEE Trans. Microw. Theory Tech.* **2014**, *62*, 513–520. [CrossRef]
10. Ahsan, S.A.; Ghosh, S.; Khandelwal, S.; Chauhan, Y.S. Modeling of kink-effect in RF behaviour of GaN HEMTs using ASM-HEMT model. In Proceedings of the IEEE International Conference on Electron Devices and Solid-State Circuits, Hong Kong, China, 3–5 August 2016; pp. 426–429.
11. Ahsan, S.A.; Ghosh, S.; Khandelwal, S.; Chauhan, Y.S. Pole-zero approach to analyze and model the kink in gain-frequency plot of GaN HEMTs. *IEEE Microw. Wirel. Comp. Lett.* **2017**, *27*, 266–268. [CrossRef]
12. Crupi, G.; Raffo, A.; Vadalà, V.; Avolio, G.; Schreurs, D.M.M.-P.; Vannini, G.; Caddemi, A. Technology-independent analysis of the double current-gain peak in millimeter-wave FETs. *IEEE Microw. Wirel. Comp. Lett.* **2018**, *28*, 326–328. [CrossRef]
13. Crupi, G.; Raffo, A.; Vadalà, V.; Vannini, G.; Caddemi, A. Current-gain in FETs beyond cut-off frequency. *Microw. Opt. Technol. Lett.* **2018**, *60*, 3019–3023. [CrossRef]
14. Shohat, J.; Robertson, I.D.; Nightingale, S.J. Investigation of drain-line loss and the $S_{22}$ kink effect in capacitively coupled distributed amplifiers. *IEEE Trans. Microw. Theory Tech.* **2005**, *53*, 3767–3773. [CrossRef]
15. Gao, H.; Sun, X.; Hua, Y.; Zhang, X.; Wang, R.; Li, G.P. A composite transistor to suppress kink phenomenon in HBTs for broadband design. *IEEE Electron. Device Lett.* **2010**, *31*, 1113–1115. [CrossRef]
16. Grinberg, A.A.; Luryi, S. Coherent transistor. *IEEE Trans. Electron. Dev.* **1993**, *40*, 1512–1522. [CrossRef]
17. Luryi, S.; Xu, J.; Zaslavsky, A. *Future Trends in Microelectronics Reflections on the Road to Nanotechnology*; Kluwer Academic Publishers: Dordrecht, The Netherlands, 1996.
18. Jorke, H.; Schafer, M. Resonance phase operation of bipolar transistors. In Proceedings of the IEEE Topical Meeting on Silicon Monolithic Integrated Circuits in RF Systems, Garmisch, Germany, 11 April 2003; pp. 26–28.
19. Kasper, E.; Eberhardt, J.; Jorke, H.; Luy, J.-F.; Kibbel, H.; Dashiell, M.W.; Schmidt, O.G.; Stoffel, M. SiGe resonance phase transistor: Active transistor operation beyond the transit frequency $f_T$. *Solid State Electron.* **2004**, *48*, 837–840. [CrossRef]
20. Heim, S.; Wanner, R.; Stoffel, M.; Kasper, E. Resonance phase operation of a SiGe HBT. *Mat. Sci. Semic. Proc.* **2005**, *8*, 319–322. [CrossRef]
21. Cressler, J.D. *Silicon Heterostructure Devices*; CRC Press, Taylor and Francis Group: Boca Raton, FL, USA, 2008.
22. Trew, R.J. Wide bandgap semiconductor transistors for microwave power amplifiers. *IEEE Microw. Mag.* **2000**, *1*, 46–54. [CrossRef]
23. Colantonio, P.; Giannini, F.; Giofrè, R.; Limiti, E.; Serino, A.; Peroni, M. AC-band high-efficiency second-harmonic-tuned hybrid power amplifier in GaN technology. *IEEE Trans. Microw. Theory Tech.* **2006**, *54*, 2713–2722. [CrossRef]
24. Marinković, Z.; Crupi, G.; Caddemi, A.; Avolio, G.; Raffo, A.; Marković, V.; Vannini, G.; Schreurs, D.M.M.-P. Neural approach for temperature dependent modeling of GaN HEMTs. *Int. J. Numer. Model.* **2015**, *28*, 359–370. [CrossRef]

25. Quaglia, R.; Camarchia, V.; Pirola, M.; Ghione, G. GaN Monolithic power amplifiers for microwave backhaul applications. *Electronics* **2016**, *5*, 25. [CrossRef]
26. Alim, M.A.; Rezazadeh, A.A.; Gaquiere, C. Temperature effect on DC and equivalent circuit parameters of 0.15-µm gate length GaN/SiC HEMT for microwave applications. *IEEE Trans. Microw. Theory Tech.* **2016**, *64*, 3483–3491. [CrossRef]
27. Jarndal, A.; Kouki, A. Efficient modeling of GaN HEMTs for linear and nonlinear circuits design. *Int. J. Numer. Model.* **2017**, *30*, e2100. [CrossRef]
28. Wen, Z.; Xu, Y.; Wang, C.; Zhao, X.; Chen, Z.; Xu, R. A parameter extraction method for GaN HEMT empirical large-signal model including self-heating and trapping effects. *Int. J. Numer. Model.* **2017**, *30*, e2137. [CrossRef]
29. Ramella, C.; Piacibello, A.; Quaglia, R.; Camarchia, V.; Pirola, M. High efficiency power amplifiers for modern mobile communications: The load-modulation approach. *Electronics* **2017**, *6*, 96. [CrossRef]
30. Foundry Process Data Sheet. Ref.: 170112_DS GaN GH25 Process_7012, United Monolithic Semiconductors, Villebon-sur-Yvette, France. Available online: https://www.ums-gaas.com/wp-content/uploads/2017/05/PPH25X.pdf (accessed on 15 October 2018).
31. Floriot, D.; Brunel, V.; Camiade, M.; Chang, C.; Lambert, B.; Ouarch-Provost, Z.; Blanck, H.; Grunenputt, J.; Hosch, M.; Jung, H.; Splettstober, J.; Meiners, U. GH25-10: New qualified power GaN HEMT process from technology to product overview. In Proceedings of the 9th European Microwave Integrated Circuits Conference, Rome, Italy, 6–7 October 2014; pp. 225–228.
32. Camarchia, V.; Colantonio, P.; Giannini, F.; Giofrè, R.; Jiang, T.; Pirola, M. A design strategy for AM/PM compensation in GaN Doherty power amplifiers. *IEEE Access* **2017**, *5*, 22244–22251. [CrossRef]
33. Gonzalez, G. *Microwave Transistor Amplifiers Analysis and Design*; Prentice-Hall: Upper Saddle River, NJ, USA, 1996.
34. Crupi, G.; Schreurs, D.M.M.-P.; Caddemi, A. Effects of gate-length scaling on microwave MOSFET performance. *Electronics* **2017**, *6*, 62. [CrossRef]
35. Dambrine, G.; Cappy, A.; Heliodore, F.; Playez, E. A new method for determining the FET small-signal equivalent circuit. *IEEE Trans. Microw. Theory Tech.* **1988**, *36*, 1151–1159. [CrossRef]
36. Tayrani, R.; Gerber, J.E.; Daniel, T.; Pengelly, R.S.; Rhode, U.L. A new and reliable direct parasitic extraction method for MESFETs and HEMTs. In Proceedings of the 1993 23rd European Microwave Conference, Madrid, Spain, 6–10 September 1993; pp. 451–453.
37. Jarndal, A.; Kompa, G. An accurate small-signal model for AlGaN-GaN HEMT suitable for scalable large-signal model construction. *IEEE Microw. Wirel. Comp. Lett.* **2006**, *16*, 333–335. [CrossRef]
38. Crupi, G.; Caddemi, A.; Schreurs, D.M.M.-P.; Dambrine, G. The large world of FET small-signal equivalent circuits. *Int. J. RF Microw. Comput.-Aided Eng.* **2016**, *26*, 749–762. [CrossRef]
39. Wen, Z.; Xu, Y.; Wang, C.; Zhao, X.; Xu, R. An efficient parameter extraction method for GaN HEMT small-signal equivalent circuit model. *Int. J. Numer. Model.* **2017**, *30*, e2127. [CrossRef]